Eur. Phys. J. D (2023) 77:138
https://doi.org/10.1140/epjd/s10053-023-00723-4

THE EUROPEAN PHYSICAL JOURNAL D

Regular Article – Optical Phenomena and Photonics

Tests of optical vortex detection based on the Talbot effect at fractional Talbot lengths and with grating rotation: realization for practical uses

Jirapat Janpool[1,2], Pissunee Deechuen[1,2], Sorakrai Srisuphaphon[1,2], Sitti Buathong[1,2], and Sarayut Deachapunya[1,2,a]

[1] Department of Physics, Faculty of Science, Burapha University, Sean Suk, ChonBuri Province 20131, Thailand
[2] Quantum and Nano Optics Research Unit, Burapha University, Sean Suk, ChonBuri Province 20131, Thailand

Received 31 March 2023 / Accepted 3 July 2023 / Published online 15 July 2023

Abstract. The optical vortex (OV) beam which has orbital angular momentum states was detected using the Talbot effect. The results clearly demonstrated the identification of the order and charge of the vortices. However, this technical detection was performed at the Talbot length and multiples thereof. This detection technique is now extended to fractional Talbot lengths. The results confirm that the best measurement contrast is still at periodic multiples of the Talbot length. In addition, the grating rotation has been realized. The grating rotation, that is, the rotation of the interference fringes, has no effect on the tilted dark stripes used to determine the order and charge of the OV beam. The direction of the tilted dark stripes is still aligned with the interference patterns. This makes the Talbot detection method more convenient and flexible for uses in optical applications.

1 Introduction

In physical nature, vortices are often described as a particular area encircled by some physical variables; they can be observed in tropical cyclones, water whirlpools, solar plasmas, spiral galaxies, and even quantum fluids. In 1989, vortices of light were first suggested by Coullet et al., sharing some similarities with vortex beams in superfluids [1]. Allen et al. later demonstrated that optical vortices in the Laguerre-Gaussian (LG) modes could carry orbital angular momentum (OAM), which was explained by an azimuthal phase factor $\exp(i\ell\theta)$, where ℓ is the integer topological charge [2]. Since then, vortex beams of light have been pursued in a board range of promising applications including optical communication [3], biological microscopy [4,5], optical manipulation [6,7], and optical metrology [8–10].

The characterization of optical OAM beams with different topological charges has been the subject of much research interest, focusing on the essences in using optical vortices. In the recent years, various techniques for investigating vortex light have been proposed involving interference patterns, such as Sagnac and lateral shearing interferometers with the common path setups [11,12], Moiré refractometry [13,14] and an inverted field interferometer [15] for detecting short pulses of vortex light. Probing with weak random scattering screen was reported [16]. The Sagnac interferometer was also utilized in studying OAM light of a single photon [17]. Phase-shifting interferometry and interferometry without an external reference light beam were demonstrated in measuring vortex beams with interferograms for fast detection [18,19]. Interference fringes from Newton's rings could be experimentally exploited in determining topological charges [20]. Furthermore, identification of vortex number was achieved using diffractive elements, such as diverse types of apertures [21–26] and gratings [27–30].

It was also shown that the Talbot effect, the self-imaging of an optical grating resulting from near-field Fresnel diffraction [31], could be employed for studying and distinguishing optical vortices using typical diffraction gratings [32–37]. The signatures of the vortex topological numbers were normally identified via examining the dark stripes on the Talbot diffraction patterns recorded at the Talbot length. Other works using two-dimensional amplitude gratings for OAM determination were associated with inspection of the Talbot carpets [38–41]. Three-dimensional optical vortex lattices were also calculated numerically by Fresnel diffraction [42].

Here, we report on a detailed study extending the former works [32,33,37] to examine the Talbot effects of optical vortices from two overlapping gratings at different Talbot planes, placed at fractional and multiple Talbot distances, and at different grating rotation angles. Experimental data were analyzed with the aid

[a] e-mail: sarayut@buu.ac.th (corresponding author)

of simulations based on the Fresnel approximation to validate the key findings.

2 Theory and methodology

Figure 1 illustrates the context for theoretical consideration. From left to right, an incoming wave with an optical vortex propagates along the z-axis. Diffraction through the gratings G_1 and G_2 with grating period d produces the interference pattern of the Talbot effect [34]. Nevertheless, the diffraction with two gratings can be represented as a single grating by setting the space between the two gratings to $L_T = d^2/\lambda$, where λ is the source wavelength. Both gratings have to align parallel to each other in order to fulfil this condition. This setup provides the near-field interference pattern as a single grating with a smaller effective open fraction $f_{eff} = \delta/d$, with a transverse shift δ. Therefore, according to the Fresnel integral, the wave function behind G_2 is given by

$$\psi_{\pm\ell}(x, y, z, \theta) = \hat{F}(x, y, z; x_1, y_1, 0) T_G(x_1, y_1, \theta) V_{\pm\ell}(x_1, y_1, z_1 = 0), \quad (1)$$

where $\hat{F}$ represents the transition operator with the Fresnel approximation for propagation from $(x_1, y_1, 0)$ to (x, y, z),

$$\hat{F}(x, y, z; x_1, y_1, 0) \equiv \frac{ik\, e^{-ikz}}{2\pi z} \int_{-\infty}^{\infty} dx_1 \int_{-\infty}^{\infty} dy_1 \exp\left\{\frac{-ik}{2z}((x - x_1)^2 + (y - y_1)^2)\right\}, \quad (2)$$

with $k = 2\pi/\lambda$. The grating transmission function

$$T_G(x_1, y_1, \theta) = \sum_n A_n \exp\{ink_d(x_1 \cos\theta + y_1 \sin\theta - \delta)\}, \quad (3)$$

has the Fourier components $A_n = \sin(n\pi f_{eff})/n\pi$ with an effective open fraction f_{eff} and $k_d = 2\pi/d$. The rotational angle θ about z-axis of the gratings has been utilized in the transformed coordinate $x_1 \cos\theta + y_1 \sin\theta$. The transverse shift δ is added to obtain the small effective open fraction $f_{eff} < 0.5$ by overlapping gratings [35]. We use the optical vortex wave function in the Gaussian form

$$V_{\pm\ell}(x_1, y_1, z_1 = 0) = (x_1 \pm iy_1)^{|\ell|} \exp\{(-1/w^2)(x_1^2 + y_1^2)\}, \quad (4)$$

for an orbital state $\pm\ell$ with the Gaussian radius w. To do the integration in Eq. (1), we apply the identity $(-i)^\ell(\frac{\partial}{\partial X} \pm i\frac{\partial}{\partial Y})^\ell \exp\{i(x_1 X + y_1 Y)\} = (x_1 \pm iy_1)^\ell \exp\{i(x_1 X + y_1 Y)\}$ [32] by substituting $X =$

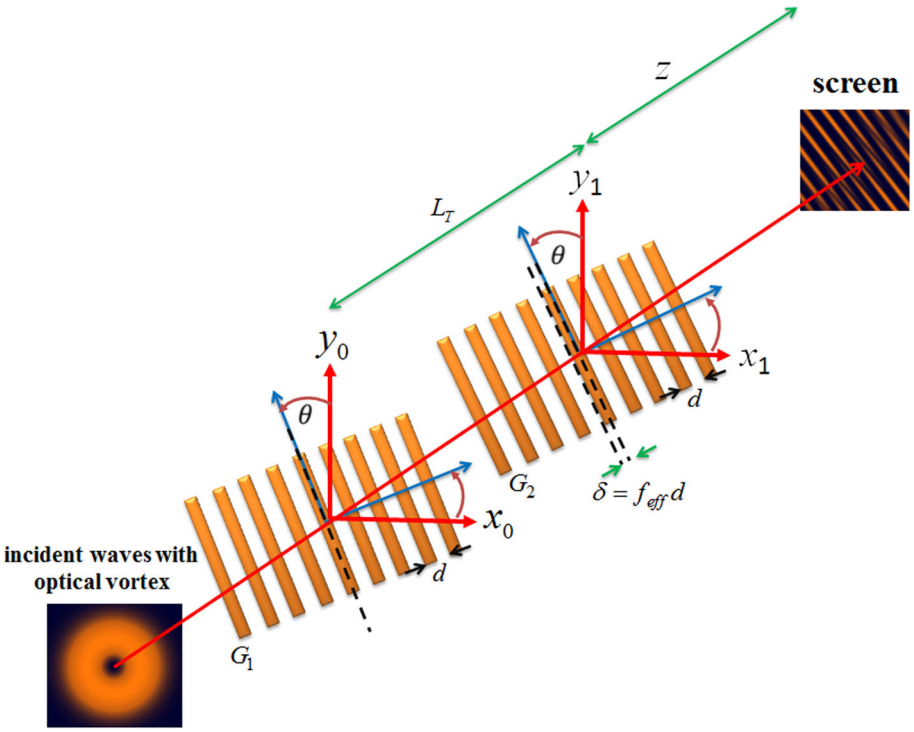

Fig. 1 Sketch of the Talbot detection of the OV beam at fractional Talbot distances with grating rotation

$(kx/z)+nk_d\cos\theta$ and $Y=(kx/z)+nk_d\sin\theta$. The integral can be evaluated and yields the exact wave function

$$\psi_{\pm\ell}(x,y,z,\theta)=\left(\frac{ik}{2Cz}\right)^{\ell+1}\exp\left\{-ikz-\frac{ik}{2z}(x^2+y^2)\right\}\sum_n A_n\left(x_n(\theta)\pm iy_n(\theta)\right)^{|\ell|}\exp\left\{\left(-\frac{k^2}{4Cz^2}\right)\left[x_n^2(\theta)+y_n^2(\theta)\right]\right\},\quad(5)$$

where

$$x_n(\theta)=x+\frac{nk_dz}{k}\cos\theta,\ \ y_n(\theta)=y+\frac{nk_dz}{k}\sin\theta,\quad(6)$$

and $C=\frac{1}{w^2}+\frac{ik}{2z}$. The theoretical simulations of $|\psi_{\pm\ell}(x,y,z,\theta)|^2$ correspond to intensity patterns discussed in the following section.

3 Experimental setup

Experimental investigations are based on the setups shown in Fig. 2. Here, we explain briefly the experimental setups (details of similar setups are shown elsewhere [37]). A 780 nm laser diode (LD, L785H1, Thorlabs) was used as the light source, and the light was expanded to cover the gratings (binary grating with d =200 μm, chromium on glass, Edmund Optics Inc.) by using a home-made beam expander (BE). A polarizer (LP, LPVIS100-MP2, Thorlabs) constrains the linear polarization of the laser beam and a quarter-wave plate (QWP, WPQ10M-780, Thorlabs) was then used to transform this linear polarized light to a circularly polarized light, with both left- or right-handed circular polarizations by rotating the polarizer. The circular polarization states are required for the OV beam production using a VHWR (VHWR, WPV10L-780, Thorlabs). The left-handed circular polarization (LHCP) generates the OV beam with $+\ell$, and the right-handed circularly polarized (RHCP) light will provide -ℓ. We used the Talbot effect [31,43] for the vortex detection [32,33] and the technique of two overlapping gratings [34,35] for an arbitrary open fraction was applied to optimize the interference contrast. The translation stages (S1, and S in Fig. 2, XR25C/M, Thorlabs) can be used to adjust the open fraction by moving the second grating (G_2) transversely. The Talbot patterns were used to measure the order and sign of the OV beam

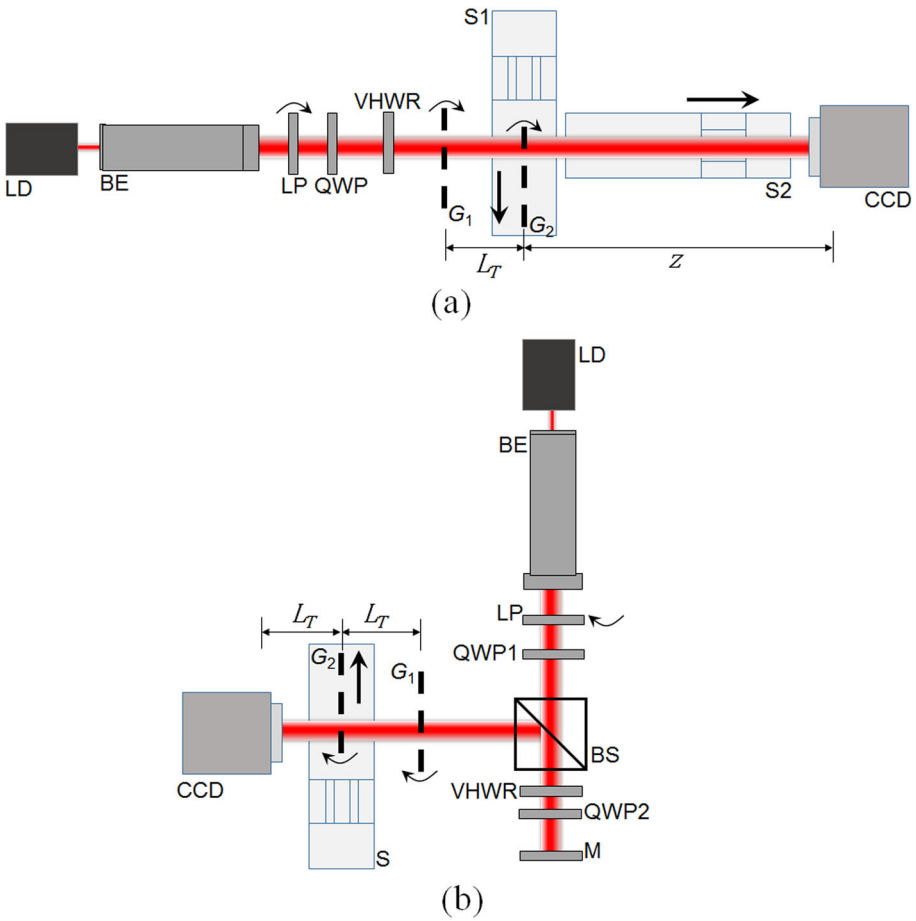

Fig. 2 Experimental setups for testing the idea: Talbot detection at fractional Talbot lengths and grating rotation with $l=\pm1$ (**a**), and $l=\pm2$ (**b**). Please see the text for details

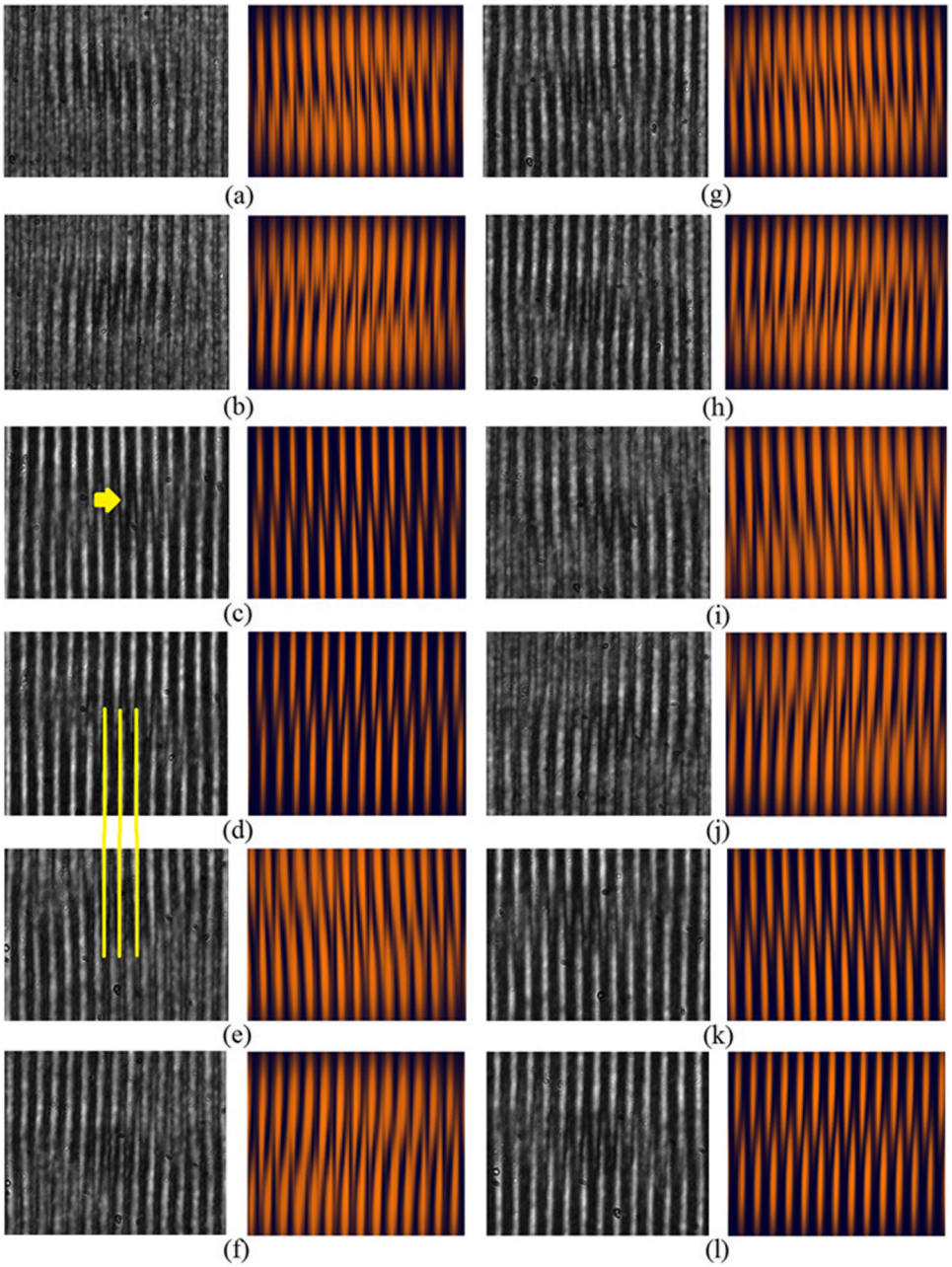

Fig. 3 Talbot detection using $d = 100\mu$m, and $f_{eff} = 0.32$ with the conditions **a** $z = 3.25L_T$, $l = +1$, **b** $z = 3.25L_T$, $l = -1$, **c** $z = 4L_T$, $l = +1$, **d** $z = 4L_T$, $l = -1$, **e** $z = 4.75L_T$, $l = +1$, (f) $z = 4.75L_T$, $l = -1$, **g** $z = 3.75L_T$, $l = +1$, **h** $z = 3.75L_T$, $l = -1$, (i) $z = 4.25L_T$, $l = +1$, **j** $z = 4.25L_T$, $l = -1$, **k** $z = 5L_T$, $l = +1$, and **l** $z = 5L_T$, $l = -1$. In each picture on the left is the experiment, and on the right is the numerical simulation of $I = |\psi_{\pm\ell}(x, y, z, \theta)|^2$ with $w = 6d$. The arrow points in **c**, as an example, at the tilted single dark stripe inclined to the left, indicated for $l = +1$. The three vertical lines, as an example, from **d** to **e** indicate to compare the patterns at the same lines from the Talbot effect to fractional Talbot effect (**d**, **e**)

from the recorded images. These images were recorded by a CCD (MT9J003 1/2.3-inch 10 Mp CMOS). The translation stage (S2 in Fig. 2a, PT1/M-Z8, Thorlabs) was used to adjust the distance of the CCD camera behind the second grating (G_2) in order to determine a proper distance for Talbot detection of the OV beam. For the study of grating rotation, the first and second gratings were simultaneously rotated for equal angles to set the Talbot pattern to always have the same open fraction. The demonstration was extended to $l = \pm 2$ according to the setup in Fig. 2b. The double-pass configuration [37] was utilized for this purpose. A beam splitter (BS, BS017, Thorlabs) and mirror (M, BB1-E03, Thorlabs) provide the double-pass transmission

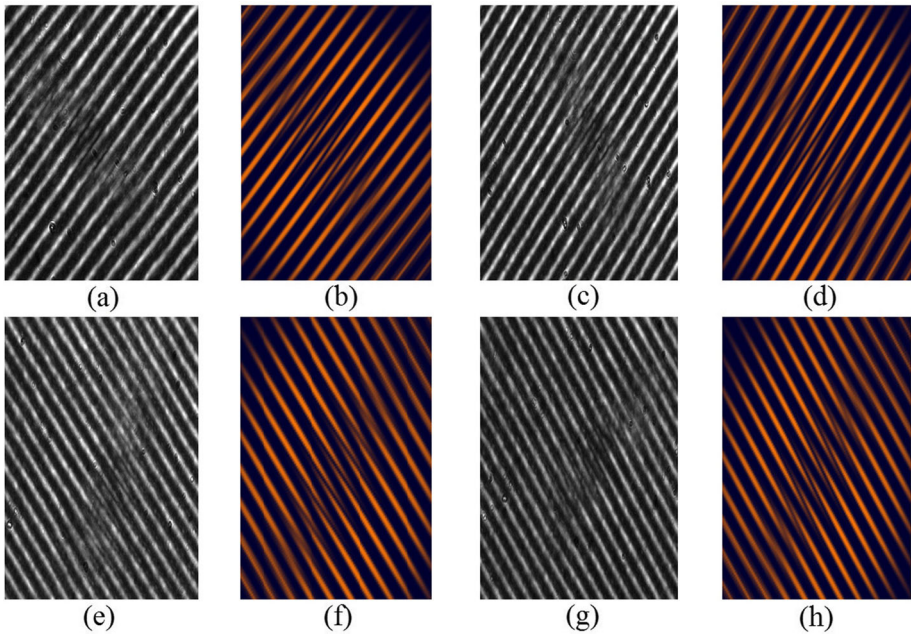

Fig. 4 Results taken at the $z = 4L_T$, $d = 100\mu$m, and $f_{eff} = 0.32$ with the conditions **a** $l = +1$, $\theta = -45°$, **c** $l = -1$, $\theta = -45°$, **e** $l = +1$, $\theta = +45°$, and **g** $l = -1$, $\theta = +45°$ experimentally. The conditions **b**, **d**, **f**, and **h** present simulation results in the same order as the experimental results

through the VHWR plate. The second quarter-wave plate (QWP2, WPQ10M-780, Thorlabs) transforms the polarization of the beam back to the initial polarization state as produced behind the first quarter-wave plate (QWP1, WPQ10M-780, Thorlabs) because the VHWR changes the circular polarization state to the opposite value when light enters the VHWR plate.

4 Results and discussion

We have proposed the idea of using the Talbot effect as a vortex detection method. Therefore, in this recent work, we optimized the detection distance behind the diffraction grating. The distances were varied at some distances of particular interest between $z = 3.25L_T$ and $z = 5L_T$ with both OV beams having $l = +1$ and $l = -1$. These distances were fractional Talbot distances. The results in Fig. 3 show that the best position for detecting the OV beam was at the Talbot distance and multiples of it, giving high contrast in the interference pattern, and also the tilt of dark stripe (the arrow in Fig. 3c) was used to identify the OAM states that can be obtained (Fig. 3c, d, k, and l). Next, we addressed an important issue. This Talbot detection method relies on the direction and number of the tilted dark stripes appearing at the middle of the OV beam in the Talbot pattern. It was necessary to confirm that the direction of the tilted dark stripes is really aligned within the Talbot interference pattern and also rotates with this interference pattern in such a way that it does not lead to misunderstanding of the charge or sign of ± of the OAM of the OV beam. For doing this, we rotated the diffraction gratings to different angles $\theta = \pm 45°$. The results for $l = \pm 1$ and $l = \pm 2$ are shown in Figs. 4 and 5. This ensures that no matter whether the grating is misaligned or tilted, this method can identify and separate the OAM states accurately. Moreover, our theoretical approach can predict our experimental results nicely. They are perfectly consistent mutually. This Talbot detection is very simple and practical. This technique uses only a few optical elements such as a diffraction grating and a camera. We therefore confirm that this technique will be a practical alternative technique for applications in vortex detection and characterization.

5 Conclusion

In this recent work, we present novel techniques in using the Talbot effect for the OV beam detection. We extended our prior study results by performing detection at fractional Talbot distances and at various angles of the diffraction gratings, to optimize the image contrast and the identification of the OAM states, respectively. In addition, this optical carpet with imprinted optical vortex beam can be considered as possible 3D optical lattice. Our experimental results and simulations confirm that this Talbot detection is very simple and practical. This makes the method more convenient and flexible for optical applications, such as in optical communications and imaging.

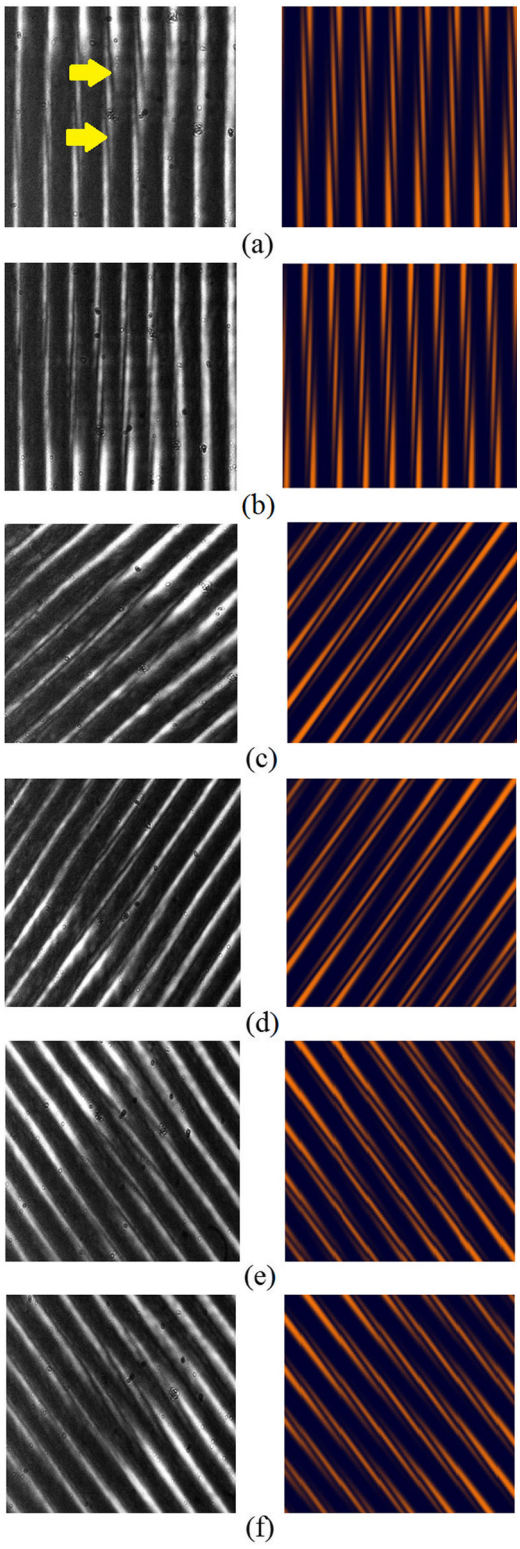

Fig. 5 Results taken at the $z = 1L_T$, $d = 200\mu$m, and $f_{eff} = 0.19$ with the conditions **a** $l = +2$, $\theta = +0°$, **b** $l = -2$, $\theta = +0°$, **c** $l = +2$, $\theta = -45°$, **d** $l = -2$, $\theta = -45°$, **e** $l = +2$, $\theta = +45°$, and **f** $l = -2$, $\theta = +45°$. The experimental results stand on the left and the calculation results are opposite to them. The arrows point in **a** for example, at the tilted dark stripes, where two dark stripes are inclined to the left, indicating that $l = +2$

Author contributions

Conceptualization: [SS, SB, SD]; Methodology: [JJ, PD]; Writing - original draft preparation: [SS, SB, SD]; Funding acquisition: [SD]; Supervision: [SD].

Funding The research unit grants from the Faculty of Science and Burapha University (RU01/2565); (i) Burapha University (BUU), (ii) Thailand Science Research and Innovation (TSRI), and (iii) National Science Research and Innovation Fund (NSRF) (Fundamental Fund: Grant No.40.1/2566); Office of the Permanent Secretary, Ministry of Higher Education, Science, Research and Innovation (OPS MHESI), Thailand Science Research and Innovation (TSRI) and Burapha University (Grant No. RGNS 65-128).

Data Availability Statement This manuscript has no associated data or the data will not be deposited. [Authors' comment: The datasets generated during and/or analysed during the current study are available from the corresponding author on reasonable request].

References

1. P. Coullet, L. Gil, F. Rocca, Optical vortices. Opt. Commun. **73**, 403–408 (1989)
2. L. Allen, M.W. Beijersbergen, R.J.C. Spreeuw, J.P. Woerdman, Orbital angular momentum of light and the transformation of Laguerre-Gaussian laser modes. Phys. Rev. A **45**, 8185–8189 (1992)
3. M.J. Padgett, Orbital angular momentum 25 years on. Opt. Exp. **25**(10), 11265–11274 (2017)
4. K.I. Willig, S.O. Rizzoli, V. Westphal, R. Jahn, S.W. Hell, STED microscopy reveals that synaptotagmin remains clustered after synaptic vesicle exocytosis. Nature **440**(7086), 935–939 (2006)
5. F. Tamburini, G. Anzolin, G. Umbriaco, A. Bianchini, C. Barbieri, Overcoming the rayleigh criterion limit with optical vortices. Phys. Rev. Lett. **97**(16), 163903 (2006)
6. Y. Shen, X. Wang, Z. Xie, C. Min, X. Fu, Q. Liu, M. Gong, X. Yuan, Optical vortices 30 years on: OAM manipulation from topological charge to multiple singularities. Light Sci. Appl. **8**, 90 (2019)
7. Y. Yang, Y. Ren, M. Chen, Y. Arita, C. Rosales-Guzmán, Optical trapping with structured light: a review. Adv. Photon. **3**(3), 034001 (2021)
8. W. Wang, T. Yokozeki, R. Ishijima, A. Wada, Y. Miyamoto, M. Takeda, S.G. Hanson, Optical vortex metrology for nanometric speckle displacement measurement. Opt. Express **14**, 120–127 (2006)
9. S. Qiu, Y. Ren, T. Liu, L. Chen, C. Wang, Z. Li, Q. Shao, Spinning object detection based on perfect optical vortex. Opt. Lasers Eng. **124**, 105842 (2020)
10. F. Pang, L. Xiang, H. Liu, L. Zhang, J. Wen, X. Zeng, T. Wang, Review on fiber-optic vortices and their sensing applications. J. Lightwave Technol. **39**, 3740–3750 (2021)
11. D.N. Naik, N.A. Saad, D.N. Rao, N.K. Viswanathan, Ultrashort vortex from a Gaussian pulse-An achromatic interferometric approach. Sci. Rep. **7**, 2395 (2017)
12. S. Zhang, P. Li, S. Wang, J. Tan, G. Feng, S. Zhou, Ultrafast vortices generation at low pump power and

shearing interferometer-based vortex topological detection. Laser Phys. Lett. **16**, 035302 (2019)
13. M. Yeganeh, S. Rasouli, M. Dashti, S. Slussarenko, E. Santamato, E. Karimi, Reconstructing the Poynting vector skew angle and wavefront of optical vortex beams via two-channel Moiré deflectometery. Opt. Lett. **38**, 887–889 (2013)
14. S. Rasouli, M. Yeganeh, Use of a two-channel Moiré wavefront sensor for measuring topological charge sign of the vortex beam and investigation of its change due to an odd number of reflections. Int. J. Opt. Photonics **7**, 77–83 (2013)
15. N. Dimitrov, M. Zhekova, G.G. Paulus, A. Dreischuh, Inverted field interferometer for measuring the topological charges of optical vortices carried by short pulses. Opt. Commun. **456**, 124530 (2020)
16. M. Liu, Probing the vortex beams with fractional and integral topological charges using weak random scattering screen. Eur. Phys. J. D **67**, 244 (2013)
17. M. Aili, X.-X. Chen, P. Liu, J.-Z. Yang, X. Guo, J. Li, Z. Meng, Q.-Y. Wu, A.-N. Zhang, Characterizing interference effects of vortex beams based on the Sagnac interferometer. Phys. Rev. A **106**, 023715 (2022)
18. G. Rodríguez-Zurita, A.G. Calderón-Hernández, L.A. Rendón-Delgado, N.I. Toto-Arellano, D.I. Serrano-García, Single shot phase-shifting interferometry with q $= \pm 1$ optical vortices and modulation of polarization. Opt. Laser Technol. **128**, 106199 (2020)
19. P. Kumar, N.K. Nishchal, T. Omatsu, A.S. Rao, Self-referenced interferometry for single-shot detection of vector-vortex beams. Sci. Rep. **12**, 17253 (2022)
20. J. Yan, J. Yao, Y. Liu, Y. Yang, Generalized Newton's rings with vortex beams. Opt. Express **30**, 44132–44140 (2022)
21. J.P.C. Narag, N. Hermosa, Probing higher orbital angular momentum of Laguerre-Gaussian beams via diffraction through a translated single slit. Phys. Rev. Appl. **11**, 054025 (2019)
22. O. Emile, J. Emile, Young's double-slit interference pattern from a twisted beam. Appl. Phys. B **117**, 487 (2014)
23. L. Yongxin, T. Hua, P. Jixiong, L. Baida, Detecting the topological charge of vortex beams using an annular triangle aperture. Opt. Laser Technol. **43**, 1233 (2011)
24. Y. Liu, J. Pu, Measuring the orbital angular momentum of elliptical vortex beams by using a slit hexagon aperture. Opt. Commun. **284**, 2424 (2011)
25. X. Chen, A. Zhang, J. Liu, Z. Xie, M. Su, Y. He, X. Zhou, Y. Chen, Y. Li, S. Chen, Orbital angular momentum modes identification of optical vortices using binaural circular aperture. J. Opt. **21**, 065603 (2019)
26. L. Ding, Z. Meng, S. Feng, S. Nie, J. Ma, C. Yuan, Measuring the topological charge of optical vortices using elliptical airy phase mask. IEEE Photon. Technol. Lett. **32**(12), 741–744 (2020)
27. S. Zheng, J. Wang, Measuring orbital angular momentum (OAM) states of vortex beams with annular gratings. Sci. Rep. **7**, 40781 (2017)
28. P. Amiri, A.M. Dezfouli, S. Rasouli, Efficient characterization of optical vortices via diffraction from parabolic-line linear gratings. J. Opt. Soc. Am. B **37**, 2668 (2020)
29. D. Hebri, S. Rasouli, M. Yeganeh, Intensity-based measuring of the topological charge alteration by the diffraction of vortex beams from amplitude sinusoidal radial gratings. J. Opt. Soc. Am. B **35**, 724 (2018)
30. J. Wang, Z. Shao, Y. Wen, X. Qiu, Y. Chen, Y. Zhang, S. Yu, L. Chen, All-dielectric metasurface grating for on-chip multi-channel orbital angular momentum generation and detection. Opt. Express **27**, 18794 (2019)
31. H.F. Talbot, Fact relating to optical science. Phi. Mag. Ser. **9**, 401–407 (1836)
32. P. Panthong, S. Srisuphaphon, A. Pattanaporkratana, S. Chiangga, S. Deachapunya, A study of optical vortices with the Talbot effect. J. Opt. **18**, 035602 (2016)
33. P. Panthong, S. Srisuphaphon, S. Chiangga, S. Deachapunya, High-contrast optical vortex detection using the Talbot effect. Appl. Opt. **57**, 1657–1661 (2018)
34. S. Srisuphaphon, S. Buathong, S. Deachapunya, Simple technique for producing a 1D periodic intensity profile with a desired open fraction for optical sensor applications. J. Opt. Soc. Am. B **37**, 2021–2025 (2020)
35. S. Buathong, S. Srisuphaphon, S. Deachapunya, Probing vortex beams based on Talbot effect with two overlapping gratings. J. Opt. **24**, 025602 (2022)
36. S. Srisuphaphon, S. Buathong, S. Deachapunya, Realization of an optical vortex from light-emitting diode source by a vortex half-wave retarder and using Talbot effect based detection. Opt. Laser Technol. **148**, 107746 (2022)
37. S. Deachapunya, S. Srisuphaphon, S. Buathong, Production of orbital angular momentum states of optical vortex beams using a vortex half-wave retarder with double-pass configuration. Sci. Rep. **12**, 6061 (2022)
38. B. Knyazev, O. Kameshkov, N. Vinokurov, V. Cherkassky, Y. Choporova, V. Pavelyev, Quasi-Talbot effect with vortex beams and formation of vortex beamlet arrays. Opt. Express **26**, 14174–14185 (2018)
39. S. Rasouli, D. Hebri, Theory of diffraction of vortex beams from 2D orthogonal periodic structures and Talbot self-healing under vortex beam illumination. J. Opt. Soc. Am. A **36**, 800–808 (2019)
40. D.A. Ikonnikov, S.A. Myslivets, M.N. Volochaev, V.G. Arkhipkin, A.M. Vyunishev, Two-dimensional Talbot effect of the optical vortices and their spatial evolution. Sci. Rep. **10**, 20315 (2020)
41. I.A. Kotelnikov, O.E. Kameshkov, B.A. Knyazev, Diffraction of bessel beams on 2D amplitude gratings-a new branch in the talbot effect study. J. Opt. **22**, 065603 (2020)
42. D.A. Ikonnikov, S.A. Myslivets, V.G. Arkhipkin, A.M. Vyunishev, 3D optical vortex lattices. Ann. Phys. **534**(7), 2100114 (2021)
43. W.B. Case, M. Tomandl, S. Deachapunya, M. Arndt, Realization of optical carpets in the Talbot and Talbot-Lau configurations. Opt. Express **17**(23), 20966–20974 (2009)